ELSEVIER

Tectonophysics 286 (1998) 223–236

TECTONOPHYSICS

Crustal imaging in southern California using earthquake sequences

Sergio Chávez-Pérez *, John N. Louie +

Seismological Laboratory/174, Mackay School of Mines, University of Nevada, Reno, NV 89557-0141, USA

Received 2 January 1997; accepted 7 July 1997

Abstract

An inexpensive means to further understand the geometry of active faults in southern California arises from the use of aftershock recordings to image crustal structures. The advent of regional seismic networks that record digital seismograms from hundreds of stations makes this crustal reflectivity profiling possible even in the absence of conventional active-source seismic data. We show that it is feasible to image fault structure using three-dimensional, wide-angle prestack Kirchhoff migration. We achieve this with the use of aftershock traces recorded on the short-period vertical stations of the Southern California Seismic Network. This work complements seismicity and focal mechanism work by imaging reflectivity volumes and cross-sections rather than having to associate events with certain faults. Further, it can image below the seismogenic zone to resolve current geologic controversies on how proposed faults extend below focal depths. We demonstrate the validity of these images as showing reflective structures, and the ability to use clipped high-gain seismograms as sign-bit data to yield valid geometric imaging. Work with data from the 1991 Sierra Madre earthquake sequence images the prominent lower-crustal reflective zone observed beneath most of the San Gabriel Mountains by the Los Angeles Region Seismic Experiment Line 1. Aftershocks of the 1994 Northridge earthquake allow us to image a north-dipping structure that may represent the fault plane of a crustal-penetrating blind thrust. The images serve as a test for the existence and geometry of thrust ramps and detachments proposed from balanced-section reconstructions of shallow-crustal profiles and borehole data. Our results are more consistent with a thick-skinned tectonic regime in the vicinity of the Northridge earthquake, rather than a thin-skinned model.

Keywords: seismic imaging; migration; crustal structure; earthquakes; aftershocks; southern California

1. Introduction

Acoustic imaging using the tools of exploration seismology and earthquake sources allows us to produce reflection views of the crust at depths where other data are commonly not available. For instance, James et al. (1987) and Meyer and James (1987) obtained near-vertical reflection profiles in regions of shallow seismicity, and Spudich and Bostwick (1987) capitalized on the principle of seismic reciprocity to form apparent receiver arrays from earthquake clusters, allowing them to derive apparent velocity information from just a few stations recording many events.

Morales and McMechan (1990) illustrated earthquake source imaging based on finite-difference

* Corresponding author. Present address: Subdirección de Exploración y Producción, Instituto Mexicano del Petróleo, Eje Central Lázaro Cárdenas 152, Mexico, DF 07730, Mexico. E-mail: sergio@orion.expl.imp.mx

+ Corresponding author. Fax: (702) 784-1833; E-mail: louie@seismo.unr.edu

0040-1951/98/$19.00
PII S0040-1951(97)00267-9

extrapolation, and reviewed the acoustic and elastic cases. They found that, in principle, earthquake recordings allow for reconstruction of source properties, locations, and fault orientations. Also, Rietbrock and Scherbaum (1994) described numerical examples and a successful case of a well-focused acoustic image of one earthquake source.

James et al. (1987) described some of the inherent difficulties and limitations that have discouraged the use of earthquake sources for reflection imaging. Nevertheless, there has been considerable interest in passive seismic imaging in the past few years due to the expansion of regional seismic networks, which have recorded digital seismograms from hundreds of stations. For instance, analyses of scattered waves using stacking and Kirchhoff migration have proven useful in the evaluation of generalized site effects and earthquake hazard (Spudich and Miller, 1990; Spudich and Iida, 1993; Revenaugh, 1995a,b,c; Revenaugh and Mendoza, 1996), as well as in studies of crustal scatterers near small-aperture arrays (Hedlin et al., 1994) and lower-mantle heterogeneities (Lay and Young, 1996), taking advantage of a limited range of scattering angle in those data sets.

Despite this recent work, earthquake seismologists may be reluctant to believe that one can image faults successfully using only P-to-P scattering characteristics, as we do here. For instance, Aki (1992) showed that P-to-S conversion for earthquake sources is much greater than S-to-P. Thus, the dominance of S-waves in the coda of seismograms raises concern about the validity of dealing with P-to-P scattering in imaging deep-crustal reflectors. P-to-S converted waves dominate the P-wave coda for teleseismic events, and S-to-P converted waves greatly contribute to the P-coda waves of regional earthquakes (Matsumoto, 1995). Thus, the mode conversion problem is inherently troublesome in earthquake seismology, and this remains the case in seismic reflection imaging.

In the context of exploration seismology, in which sources are typically either explosive or vertical vibrators, and recording apertures are small relative to the target depths, the effects of source directivity are less crucial (Chen and McMechan, 1992) than in earthquake seismology. Crustal-scale wide-angle experiments are potentially more affected by source type because of the wider range of propagation angles involved. Source directivity differences become increasingly important at wider and wider apertures. Strong source directivity does indeed affect the imaging process, but we show that it does not hinder the reconstruction of fault geometries having reflectivities normally associated with deep-crustal structures.

As in oil industry seismic-reflection surveying, imaging of structure through high-frequency reflectivity demands high-multiplicity data, or a large number of overlapping sources and receivers. Despite the intrinsic limitations of close source spacing (within an aftershock sequence) and wide station spacing, our initial work (Chávez-Pérez and Louie, 1995) showed that a small cluster of tens of aftershocks has the spatial sampling needed to image crustal reflectors beneath the Northridge aftershock zone. In the case of the Northridge earthquake, the close spatial distribution of aftershocks illuminates structures not previously mapped at depth (e.g., Hauksson et al., 1995). A reliable velocity structure over the three-dimensional array of sources (aftershocks) and receivers (network stations) provides some of the information needed to locate crustal reflectors in cross-sections or 3-D volumes.

Locating crustal reflectors has important neotectonic implications because the proper development of earthquake scenarios for southern California requires discovering the location and character of known and still unknown fault structures (e.g., Hauksson, 1990; Shaw and Suppe, 1996). Prime examples of blind thrusts are the sources of the 1983 Coalinga, 1987 Whittier Narrows, and 1994 Northridge earthquakes in California. Seismological evidence for the Northridge mainshock fault mechanism, the focal mechanisms and the spatial distribution of aftershocks (Hauksson et al., 1995) are consistent both with thin-skinned (Davis and Namson, 1994) and thick-skinned (Huftile and Yeats, 1996) hypotheses for blind-thrust faulting in southern California.

We test the applicability of these models using aftershock recordings to obtain images of crustal structure. This work describes our crustal imaging procedure and imaged structure beneath the 1991 Sierra Madre and 1994 Northridge earthquake sequences, using aftershocks treated with simple data editing and Kirchhoff depth migration.

2. Crustal imaging method

2.1. Data selection and preprocessing

The ideal sources for performing crustal imaging would be underground explosions, due to their simple focal mechanism (Lay, 1987; Lynnes and Lay, 1989). Successful Kirchhoff summation depends upon consistent focal mechanisms or a source correction. Here, we have made no correction for the source but, for the sake of attaining coherent summations, we use only data with high-quality impulsive P-wave picks to roughly correct for sign reversals due to varying focal mechanisms and source directivity, where the scattered ray paths have takeoff angles close to the direct ray takeoff angle. (In future work, we may improve these summations by using events with the same focal mechanisms.) Our data are short-period vertical-component seismograms from the Southern California Seismic Network (SCSN) provided through the Southern California Earthquake Center (SCEC) Data Center. We use well-located, A-quality events.

Clipped and saturated records are quite common in short-period data. We regard them as sign-bit recordings (O'Brien et al., 1982) that will acquire dynamic range through Kirchhoff summation. To project a reflected wave from a seismogram to a reflector location one needs to know the time of the arrival, and be able to characterize it as having significant amplitude within the seismogram. Stacking and migration find events that have some coherency across a source–receiver array (of events in this case) and sum amplitudes to reject uncorrelated noise. We can thus obtain coherent reflections, for instance, by common midpoint stacking (Chávez-Pérez and Louie, 1995) to improve the signal-to-noise ratio, or even by simple vertical stacking. With sufficient data redundancy, stacking and migration are often able to recover geometric information.

The record sections we use comprise 200 km in epicentral distance and 30 s duration to include wide-angle reflections between first compressional (Pg) and first shear (Sg) arrivals, and we mute outside the window between the approximate Pg and Sg traveltime branches to extract only compressional arrivals, mostly some unmuted Pg, PmP and S-to-P converted energy. Imaging artifacts result from not muting correctly the direct Pg arrivals. As they have the minimum arrival time at any offset, they will contaminate the shallow part of the images. This is not too important for us as we are interested in deep, mid-crustal structures. In addition, we must include forward-scattered energy with traveltimes close to the Pg arrival time.

Despite the fact that the bulk of short-period earthquake data analyses deal with the frequency band of 1–10 Hz, we chose to retain a wider spectrum. We retain a frequency band of 1–40 Hz because the spectra of our signals show some energy above the noise level for frequencies above 10 Hz. This is also the frequency range where reflections normally associated with deep-crustal structures have predominated in active-source crustal studies (e.g., Brewer and Oliver, 1980). In addition, there is implicit low-pass filtering during the migration process, and one can always remove the effects of high-frequency noise from the images, for plotting and stacking purposes, by postmigration low-pass or dip filtering to enhance visibility and resolution. Thus, preprocessing includes bandpass filtering (1–40 Hz) and trace equalization for receiver amplitude balancing (i.e., the amplitudes are normalized so that the mean-squared amplitude over the whole trace is the same for all traces). This is roughly equivalent to energy normalization for varying magnitudes and a geometrical spreading correction.

2.2. Prestack depth migration

We carry out the search for scattering structures and reflectors, like steeply dipping faults and thrust faults, ramps, and detachments, with the assumption that these scatterers include a component that radiates isotropically (e.g., Lay, 1987; Lynnes and Lay, 1989; Revenaugh, 1995c). Under this simple assumption, which is valid for structures that form variations in Lamé parameters (Wu and Aki, 1985; Ikelle et al., 1992), the search for crustal structures becomes practical.

Ignoring the reflection angle at the image point leads to the treatment of the data as a P-to-P isotropic scattering problem. The strength of the scattered waves we image depends on Lamé parameter λ perturbations, which behave like point explosions (Wu, 1989). Forward-scattered and back-scattered

waves will have the same phase and amplitude. We thus image variations in the Lamé parameter λ due to its independence of reflection angle. This $\Delta\lambda$ imaging is as significant as impedance imaging, since it is proportional to the relationship between compressional and shear velocities. The V_p/V_s ratio is often used to estimate the lithology of subsurface rocks from sonic logs or seismic reflection profiles.

Experimental work shows wide ranges of V_p/V_s ratios within fault zones, on the basis of seismic velocity and density measurements made on samples from exhumed faults. For instance, McCaffree and Christensen (1993) showed, for the mylonite zone of the Brevard fault, that the compressional reflectivity will normally be stronger than the shear reflectivity. This stronger compressional reflectivity appears to be related to a wider distribution of compressional versus shear velocity values, creating stronger P-wave reflection coefficients and impedance variations. Hence, fault zones exhibit a ΔV_p and $\Delta\lambda$ signature that we can image.

Our depth migration method is a backprojection of assumed primary reflection amplitudes into a depth section, based on travel times through an assumed velocity model. Because the backprojection requires knowledge of the source wavelet for deconvolution by cross-correlation with each seismic trace, we roughly approximate this by cross-correlating with a boxcar function 0.5 s long, close to the central period of the reflection arrivals. The net effect of this is to smooth the migration (through low-pass filtering of the data), center the reflection pulses near zero phase, and avoid operator aliasing (Lumley et al., 1994). This filtering also minimizes phase differences arising from our lack of knowledge of focal mechanisms.

We obtain images of subsurface reflectors by summing cross-correlated data at traveltimes computed through one-dimensional velocity models, ignoring lateral velocity variations. The Kirchhoff depth migration process we use is similar to that of Louie et al. (1988). The migration is a backprojection of assumed primary reflection amplitudes into a depth section. It has been identified by Le Bras and Clayton (1988) as the tomographic inverse of the acoustic wave equation under the Born approximation in the far field, utilizing WKBJ rays for downward continuation and two-way reflection traveltime for the imaging condition. Traveltime versus distance matrices are computed from the velocity profiles with the Vidale (1988) finite-difference solution to the eikonal equation. We obtain the final depth imaging result by stacking the migrated partial images from each event.

One of the major problems in Kirchhoff depth migration is image resolution. When we apply this method to data with limited observation geometry, artifacts or false images appear and make the results difficult to interpret. In this case, sparse receiver coverage causes artifacts along elliptical trajectories in the migrated depth section. Defocusing of P-to-S and S-to-P converted energy by the P-to-P migration also contributes to image degradation, as well as upward sweeping *smiles* produced by strong noise.

To illustrate our reconstruction of scattering structures, Fig. 1 shows the southern California velocity profile of Hadley and Kanamori (1977), which we use to image a model of a dipping mid-crustal reflec-

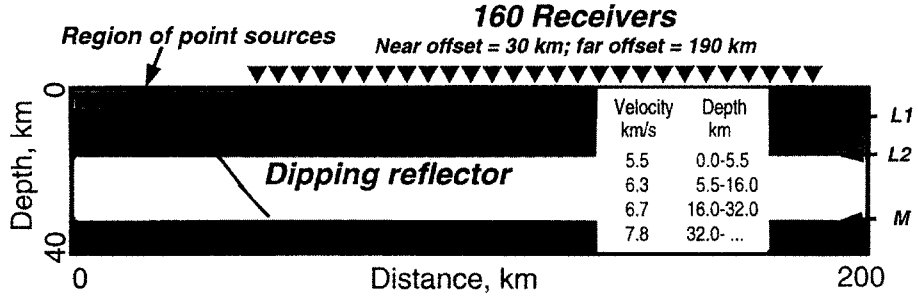

Fig. 1. Southern California velocity model used for the computation of synthetic seismograms and Kirchhoff depth imaging. The dipping reflector is the imaging target for the synthetic example and is not present in the migration velocity models. *L1*, *L2*, and *M* (Moho) stand for crustal layer interfaces.

tor from sixteen randomly placed 'earthquake' point sources. We compute synthetic record sections with the fourth-order finite-difference solution of the full-wave acoustic wave equation described by Vidale (1990). The record sections we utilize comprise up to 200 km in epicentral distance and 30 s duration to include wide-angle reflections for sixteen different source locations on a 2-D line. There is no muting or further preprocessing.

Fig. 2 shows the progressive migration of the synthetic record sections. Even the migration of seismograms from just one event (Fig. 2a) shows the crustal layering interfaces (L1, L2, and M, where M stands for the Moho). After eight events are included (Fig. 2b), the dipping structure begins to appear as well. With sixteen events, the intersections between structures are clear (Fig. 2c, white arrows), and the dipping structure is resolved. Note how apparent phase changes along the dipping reflector results from incomplete cancellation of Kirchhoff arcs that varies along its length. The input velocity model was not smoothed and contains discontinuities. Image quality could be improved, for instance, by using velocity gradients and a smoothed estimate of the velocity model. In addition, dip filtering (Hale and Claerbout, 1983) after migration may make the elliptical artifacts less distracting.

Artifacts also result from not muting the direct arrivals from the synthetic seismograms (Pg in the real seismograms). As the direct arrivals have the minimum arrival time at any offset, they backproject to the shallow part of the images. This is not too important for us as muting could improve imaging of the top of the model and we are more interested in deep structures. For the sake of illustration, note how Fig. 2c shows a light band above L1 which is due to unmuted direct arrivals. The L1 boundary, in fact, appears to have been reconstructed from forward-scattered reflections with arrival times just behind the first arrival.

The depth imaging method used in Fig. 2, backed up by more detailed velocity models than we use here, has imaged the fine structure of steeply dipping faults along with the detailed seismic stratigraphy of near-horizontal sedimentary rocks (e.g., Pullammanappallil and Louie, 1994; Chávez-Pérez et al., 1996). Picking reflections observed in the seismograms (Pullammanappallil and Louie, 1993), or an optimization based on coherency criteria without requiring picks (Pullammanappallil and Louie, 1997), can also yield highly detailed velocity results. Statistical assessments and validity checks of migrated

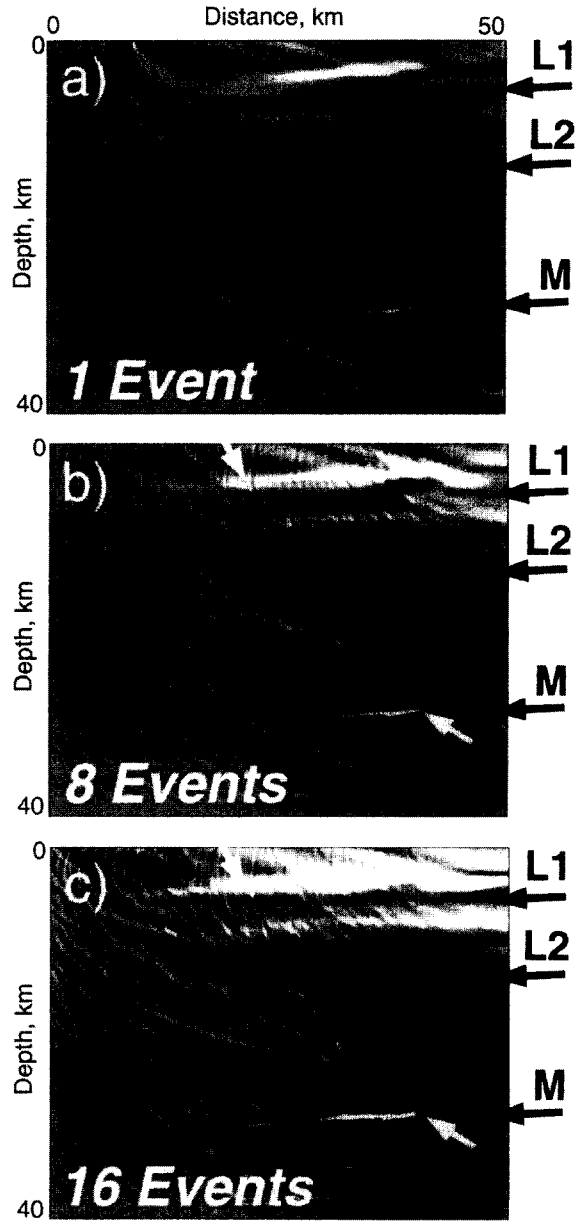

Fig. 2. Demonstration of progressive migration imaging the dipping reflector shown in Fig. 1. The reflectivity cross-sections result from Kirchhoff depth migration of progressively larger numbers of synthetic seismograms. *L1*, *L2*, and *M* (Moho) stand for crustal layer interfaces. There is no vertical exaggeration.

images, with special consideration of artifacts and resolution, can be handled in the manner of Louie and Pullammanappallil (1994).

In this study, we use signed, high-frequency seismograms from local and regional events. Our method is complementary to the work of Revenaugh (1995a,b), who has used unsigned, long-period data from similar sets of stations, and teleseisms, with a similar Kirchhoff migration method to find map-scale images of scattering property variations. In addition, Revenaugh (1995c) was able to correlate regions high in scattering potential with slip concentrations on known faults during earthquakes. While Revenaugh's (1995c) objective was to estimate a characteristic parameter on the surface of a known fault, ours is to detail the location and geometry of known and unknown faults, without providing much information on characteristic properties. He interpreted variations in regional scattering potential on a crustal scale (8–10 km), whereas we locate major structures with about 1–3 km resolution. Revenaugh (1995c) proposed likely areas of strong, frequent aftershocks, and delineated strength variations along fault systems.

3. Results

3.1. Sierra Madre earthquake sequence

Using seismic network recordings of the 1991 Sierra Madre event and its aftershocks (Hauksson, 1994), we undertook the imaging of a section through the San Gabriel Mountains near the Los Angeles Region Seismic Experiment (LARSE) Line 1, in an attempt to reproduce a lower-crustal bright spot seen by Fuis et al. (1996). The stack of explosion seismograms presented by Fuis et al. (1996) shows an outstanding, high-amplitude band of reflectivity, a 'lower crustal reflective zone' (LCRZ), at approximately 16 to 19 km (between 5.5 and 6.5 s, two-way travel time) beneath the San Gabriel Mountains, between Azusa in San Gabriel Valley and the San Andreas fault near Wrightwood, and extending about 25 km laterally (Ryberg et al., 1996).

Fig. 3 shows the locations of LARSE Line 1 and section A we used to depict a 50-km-long by 40-km-deep image of crustal structure in this region. Fig. 4 shows a representative aftershock plotted as a record section independent of azimuth. Note the azimuthal time dependence of the impulsive Pg arrivals. Fig. 5A shows the depth migration of records from eighteen events, including the Sierra Madre main shock, using the southern California velocity model of Fig. 1. The data set included as few as 18 and as many as 102 seismograms from each event, all having impulsive P-wave picks. Most of the focal mechanisms for these events show thrust faulting (Hauksson, 1994) and their depth distribution lies within 8.3–14.1 km. Datum is sea level. Brown shows positive reflectivity, white shows negative reflectivity and yellow shows small reflectivity.

To test the validity of our image, we must determine which imaged structures are real and which are artifacts produced from the imaging of noisy data. One test is a simple resampling analysis, which is done by imaging the data after destroying coherence by randomly flipping the signs of data traces. Fig. 5B depicts migration artifacts and is equivalent to migration of random noise. Compare with Fig. 5A to visually separate out artifacts from the signal of coherent reflectors. The images are most prominently different at the LCRZ. Note, for instance, how the San Andreas fault seems to extend nearly vertical through the upper crust, despite the presence of nearby imaging artifacts (Fig. 5B). However, its reflectivity is not as strong as that of the LCRZ.

Fig. 5A suggests the reflective bright spot of Fuis et al. (Fig. 5C) extends north beneath the San Andreas fault to the Mojave Desert. Our Sierra Madre migration shows, among the usual elliptical Kirchhoff migration artifacts, a strong north-dipping reflective zone at approximately 10–20 km depth below the northern side of the San Gabriel Mountains.

Fig. 5D overlays the LARSE Line 1 stack of Fuis et al. (1996) on our migration at the same scale, assuming the stack was created with accurate enough velocities to avoid vertical exaggeration, and at approximately corresponding locations. The locations of the bright spot reflector on the two sections correspond well, despite the fact that the sections are not perfectly coincident.

According to Fuis et al. (1996), the top of the lower-crustal reflective zone represents a 'block boundary', or change in rock properties, in the crustal framework of southern California. They pro-

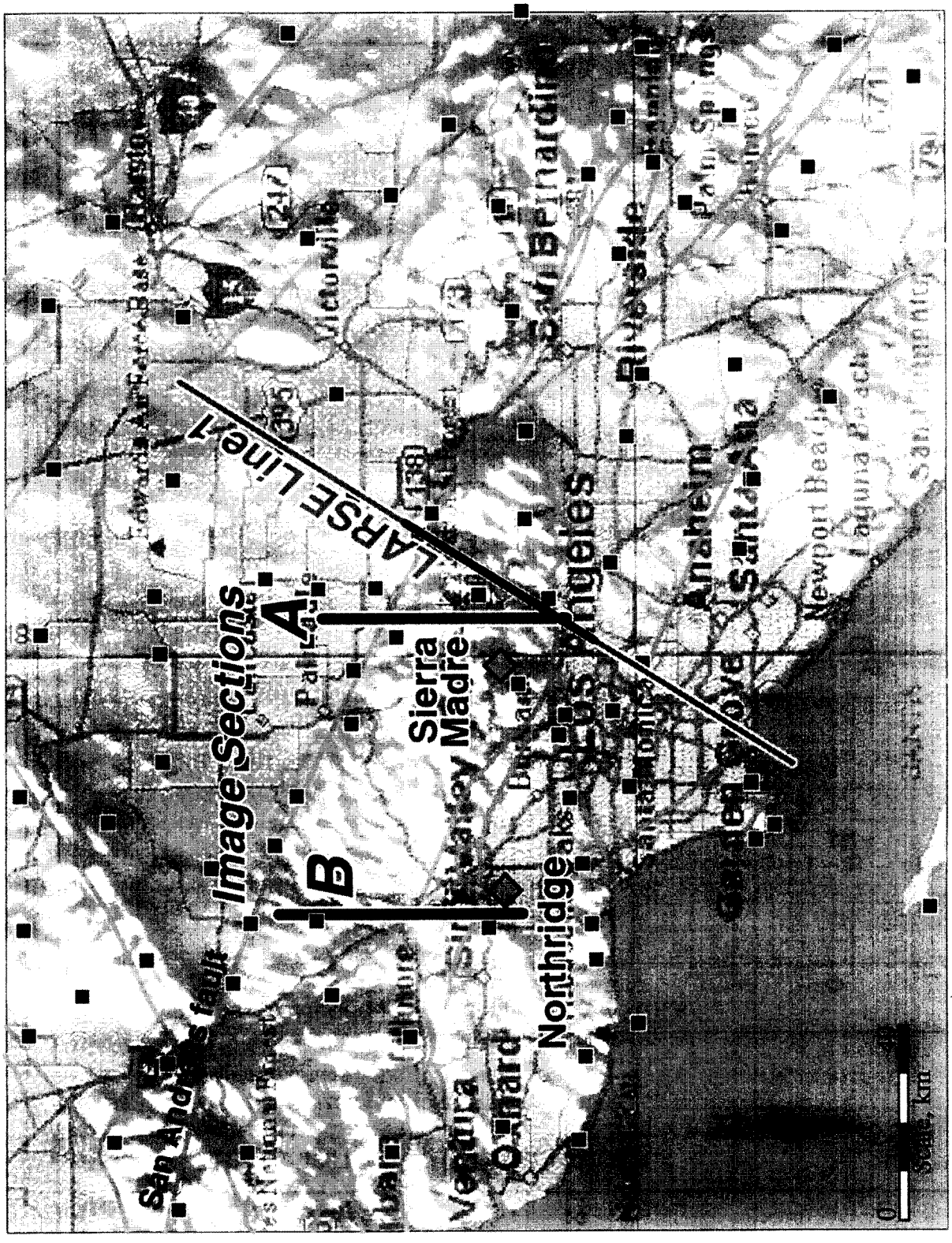

Fig. 3. Sierra Madre and Northridge main shocks (diamonds) and aftershock imaging sections (lines *A* and *B*) and the LARSE Line 1 section of Fuis et al. (1996; dark on light line) located on topography map of the Los Angeles region. Black squares show the location of some of the network stations we used.

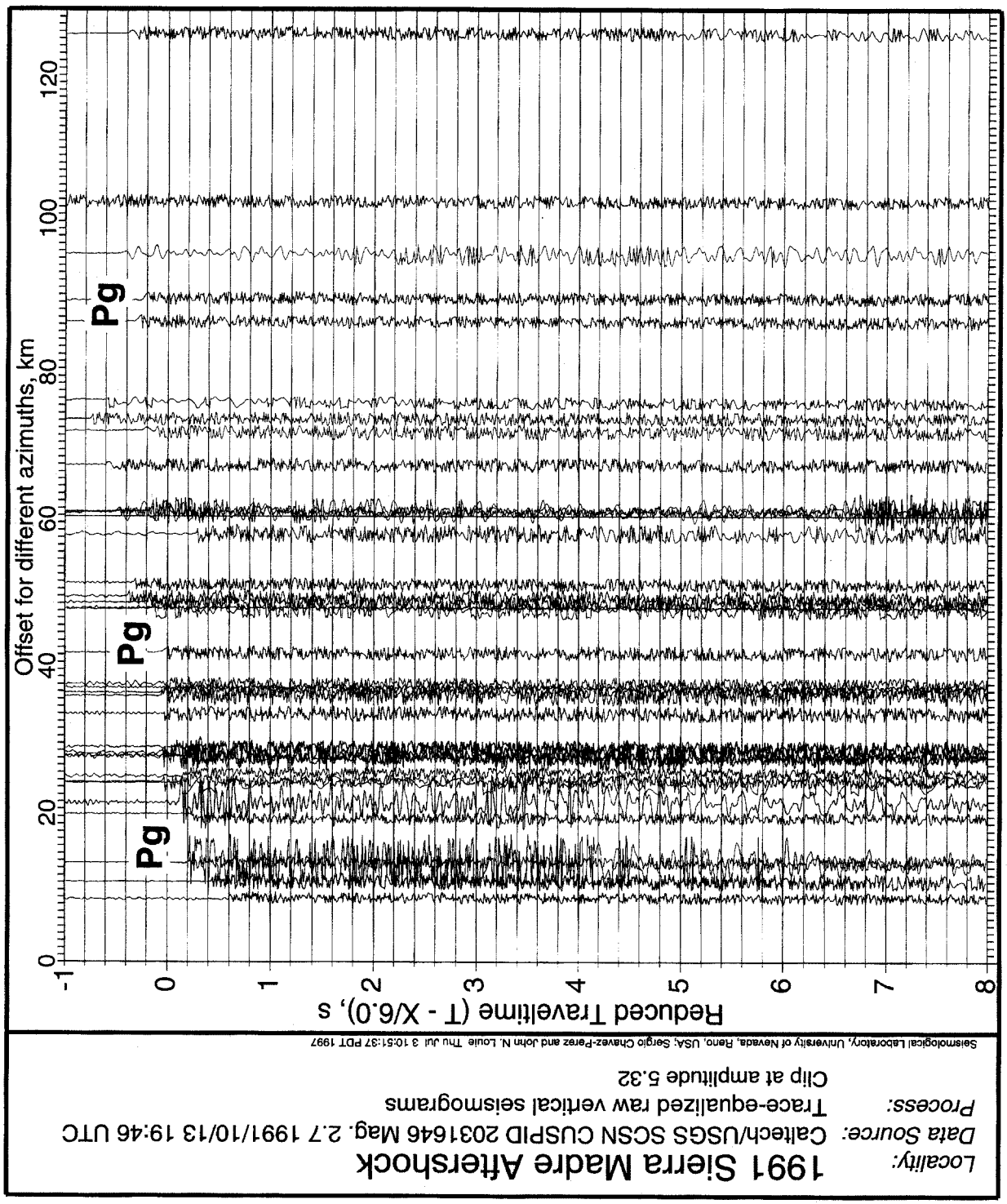

Fig. 4. Example vertical-component record section from one Sierra Madre aftershock (hypocentral depth 9.3 km). Impulsive Pg arrivals are clear. The data are plotted as a function of reduced traveltime versus offset of the recording station, independent of azimuth. Trace equalization was used for the display.

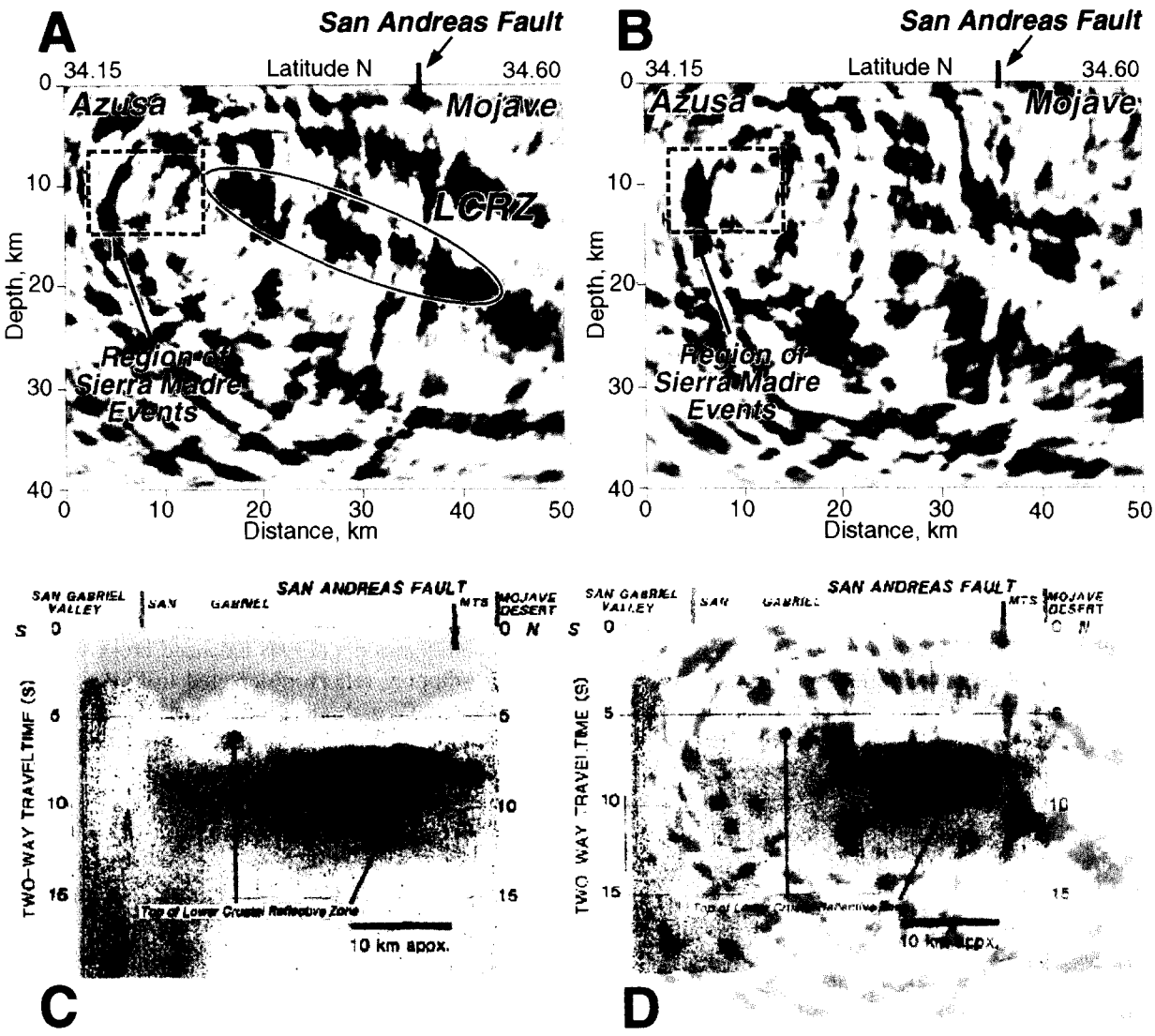

Fig. 5. (A) Depth section 50 km wide and 40 km deep from Azusa north to the margin of the Mojave Desert (Fig. 3, line A), from migration of the Sierra Madre mainshock and 17 A-quality aftershocks lying within 8.3–14.1 km of the surface. The image suggests the lower crustal reflective zone (LCRZ) of Fuis et al. (1996). (B) Depth section based on a simplified resampling analysis. This image depicts migration artifacts and is equivalent to migration of random noise. Compare with (A) to visually separate out artifacts from signal (coherent reflectors). (C) LARSE Line 1 explosion stack of Fuis et al. (1996). Note the time axis. (D) Overlay of the LARSE Line 1 explosion stack of Fuis et al. (1996) on our Sierra Madre depth section (A). Note the approximate correspondence of the main reflectors.

posed that the top may be a décollement or an intrusive contact. In fact, the depth to the brittle–ductile transition seems to be prescribed by the existence of reflective structures like this (Magistrale and Zhou, 1996). This is important, because the lateral variations in lithology seem to control the depth extents, and thus the magnitudes, of potential future earthquakes (Magistrale and Zhou, 1996). These depths, which may correlate with the presence of schist basement rocks (Pelona schist in this case), can be determined from the depth of the current background seismicity and from seismic images like those of Fig. 5A. In future work, we may improve our images by using a more reliable velocity

model (e.g., Hauksson et al., 1996), and by combining 3-D, wide-angle, prestack imaging of newly released LARSE Line 1 explosion records, together with Sierra Madre aftershock traces, through an optimized 3-D velocity model. We could then extend our analysis to the LARSE Line 1 explosion and offshore–onshore records, and the Whittier Narrows aftershock records to the south across the Elysian Park fault system in the 1987 event area (Hauksson, 1990).

3.2. Northridge earthquake sequence

A major debate in the Los Angeles basin region, analogous to that commonly found in deep seismic profiling (e.g., Cook and Varsek, 1994), has centered around the question of whether blind thrust faults maintain a constant dip and thus penetrate into deep basement ('thick skin tectonics'), or whether such faults flatten above or into a regional, subhorizontal detachment horizon, or décollement, above or high in the basement ('thin skin tectonics'). Seismological evidence for the Northridge mainshock faulting, the focal mechanism, and the spatial distribution of aftershocks (Hauksson et al., 1995) together with geological and geodetic constraints (Donnellan et al., 1993), are consistent with both 'thin-' (Davis and Namson, 1994) and 'thick-skinned' (Yeats, 1993; Huftile and Yeats, 1996) hypotheses for blind-thrust faulting in southern California.

One way to test these alternative models is to use aftershock recordings to attain crustal images. This is needed because the 'thin-' and 'thick-skinned' interpretations of the 1994 Northridge earthquake are especially dependent on accurate characterization of complex fault geometries (Mori et al., 1995). Using the techniques of Suppe and Medwedeff (1984) to model for local well and geologic data, Davis and Namson (1994) proposed a model of thrust ramps along blind thrusts below San Fernando Valley. We can test this model using crustal reflection images. Fig. 6A shows an imaged crustal section 50 km wide and 40 km deep that extends north from the Northridge epicentral area (Fig. 3, line B). The imaging utilizes the southern California velocity model of Fig. 1 and 823 wide-angle seismograms having high-quality impulsive P-wave picks from 27 shallow Northridge aftershocks. Nearly all of the focal mechanisms for these events show thrust faulting (Hauksson et al., 1995) and their depth distribution lies above 3 km. Datum is sea level. Black shows positive reflectivity, white shows negative reflectivity and gray shows little reflectivity.

Strong, north-dipping reflectors, and one south-dipping reflector, in Fig. 6A do not follow the trajectories defined by the artifacts of Fig. 6B. They correlate closely with Davis and Namson's (1994) interpreted positions of the Pico and Elysian Park thrusts, but the reflectors extend below the projected depth of their proposed mid-crustal detachment. Fig. 6B displays migration artifacts and is equivalent to migration of random noise in the same manner as that in Fig. 5B. Note how the prominent north-dipping fault system and the south-dipping reflector do not appear, and therefore are not imaging artifacts. Compare with Fig. 6A to visually separate out artifacts from signal (coherent reflectors).

Fig. 6C compares our wide-angle SCSN data image with aftershock locations, and with part of Davis and Namson's (1994) balanced cross-section. A south-dipping reflector, depicted in Fig. 6A, just below their Pico thrust may be an image of the seismogenic fault. Note that our image also shows a dipping reflector almost parallel to one of the main dipping reflectors (Elysian Park thrust).

Fig. 6D shows our interpretation of the image in Fig. 6A. It depicts faults based on coherent arrivals (as compared with Fig. 6B). Subhorizontal reflectors visible at mid-crustal depths (20 km) may be evidence for a large subhorizontal discontinuity, perhaps a detachment fault. This feature is apparently offset by the north-dipping thrust that may correspond to the Elysian Park thrust. Note that the thrust is steep, cuts the mid-crustal detachment and crust–mantle boundary (at 32 km), and appears to pass beneath the San Andreas fault and root to the north.

The presence or absence of a mid-crustal detachment in the western Transverse Ranges is a subject of current debate (Webb and Kanamori, 1985; Yeats, 1993; Davis and Namson, 1994; Huang et al., 1996; Huftile and Yeats, 1996). Huang et al.'s (1996) analysis of low-angle earthquake focal mechanisms does not support the existence of a regional-scale, seismically active detachment in southern California. Only in the western Transverse Ranges is there some suggestion of a large detachment surface at a depth of

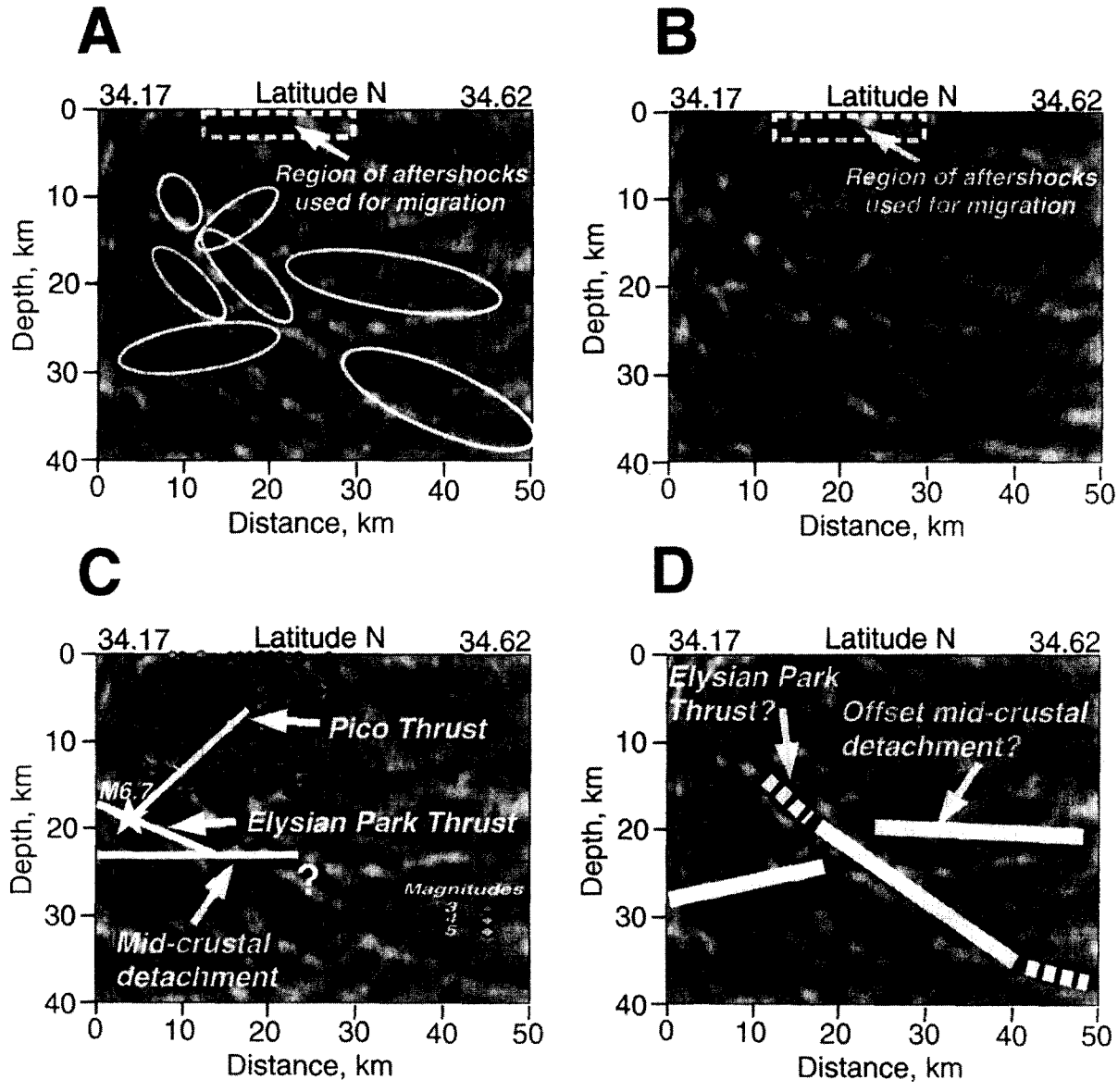

Fig. 6. (A) Crustal reflectivity below the Northridge sequence along a south–north section (Fig. 3, line B). The image has contributions from 27 A-quality aftershocks lying within 3 km of the surface. It was dip-filtered (Hale and Claerbout, 1983) to enhance the main reflectors. Note the north-dipping fault system and a south-dipping reflector. (B) Depth section based on a simplified resampling analysis. This image depicts migration artifacts and is equivalent to migration of random noise. Compare with (A) to visually separate out artifacts from signal (coherent reflectors). (C) Same image as in (A) with Northridge main shock, aftershocks and interpretations of Davis and Namson (1994) superimposed. Dipping reflectors appear that may correspond to the Pico and Elysian Park thrusts, but they extend below the projected 22-km depth of the mid-crustal detachment. (D) Same image as in (A) showing our interpretation. This is based on coherent reflections and existing geologic data. Lines suggest the approximate location of an offset mid-crustal detachment and a north-dipping fault that may correspond to the Elysian Park thrust as inferred by Davis and Namson. The Moho interface is located at 32 km.

about 13 to 14 km (Huang et al., 1996). Davis and Namson (1994) proposed that a detachment lies at a depth of about 22 km, whereas our image depicts such a detachment between 20 and 28 km. This suggests that the present crustal shortening in the region involves both the lower and upper crust.

These figures demonstrate the feasibility of obtaining interpretable structural images from wide-angle processing of aftershock data. We expect that the addition of LARSE Line 2 records and optimized 3-D velocities (Zhao and Kanamori, 1995; Magistrale et al., 1996; Hauksson and Haase, 1997) will improve structural definition and detail in the Northridge epicentral area.

4. Discussion and conclusions

The agreement between our depth section through the San Gabriel Mountains and that of the LARSE Line 1 is a positive test of our technique. It is remarkable that the narrow-angle LARSE Line 1 explosion data and the very wide-angle aftershock network records can show the same bright spot extending north from the San Gabriel Mountains area, beneath the San Andreas, into the Mojave.

This fact suggests not only that the lower crustal reflective zone is real, but also supports the accuracy of both data sets and imaging methods. Unfortunately, no other geophysical data are available to corroborate the locations of reflective structures at depths greater than 4 km, which are below the reach of petroleum industry seismic and borehole data in southern California. LARSE Line 1 results to date have provided useful information on the tectonics of southern California (Fuis et al., 1996), but have not yet shown clear structural definition of faults. However, we have shown here that it is possible to image fault geometry beneath the northern margin of the Los Angeles basin using earthquake sequences.

Our results from Northridge do not support the 'thin-skinned' interpretation of Davis and Namson (1994). Our image suggests that the main, north-dipping thrust (Elysian Park thrust?) is steep, cuts a mid-crustal detachment and the crust–mantle boundary, and appears to pass beneath the San Andreas fault and to root to the north. This thrust appears to be similar to the deeply penetrating Flannan thrust in Britain (Brewer and Smythe, 1983; Brewer et al., 1983), which, in deep reflection images, appears to cut the crust–mantle boundary.

For the last seventeen years, the literature regarding this region has been mostly in favor of the 'thin-skinned' model (e.g., Huftile and Yeats, 1995). Our interpretation is more consistent with a 'thick-skinned' tectonic regime. This suggests that the present crustal shortening in the region involves both the lower and upper crust. With this, we challenge earthquake geologists to come up with models that could create major reflectors at the locations we show.

Given the high cost of active source crustal imaging, together with the difficulty of working in heavily populated areas, our new crustal imaging technique provides a practical means to improve our understanding of the geometry of active faults in southern California. We can image thrust geometry and other structures extending into the lower crust, although data limitations will continue to be a major hurdle. The station distribution of the SCSN is inadequate to resolve faults throughout southern California; such work will be restricted to aftershock zones.

Despite the irregular distribution of SCSN stations, our depth imaging procedure uses the SCSN data in a cost-effective manner to depict the most prominent crustal structures in the region beneath two earthquake sequences. This represents, to the best of our knowledge, the first step of high-resolution imaging of complex 3-D structures with passive seismic data, using processing techniques commonly used for active crustal seismics.

Acknowledgements

This work was partly funded by a U.S. National Science Foundation grant (EAR-9416224). The first author acknowledges financial support by CONACyT, Mexico's National Council for Science and Technology. Aftershock data were recorded by the SCSN, which is operated jointly by the Seismological Laboratory at Caltech and the U.S. Geological Survey, Pasadena, California. We thank Katrin Hafner for giving us access to the SCSN data center. Steven Jaumé and Russell Brigham helped to obtain the Northridge data set used here. Gary Fuis challenged us to compare our work with that of LARSE Line 1. Harley Benz, Glenn Biasi, Michael Hedlin, Craig Nicholson, Mark Stirling, and David von Seggern have provided useful criticism and suggestions. We also thank Michael Simon, Tom Parsons, Richard Schweickert, and Walter Mooney for their helpful reviews.

References

Aki, K., 1992. Scattering conversions P to S versus S to P. Bull. Seismol. Soc. Am. 82, 1969–1972.

Brewer, J.A., Oliver, J.E., 1980. Seismic reflection studies of deep crustal structure. Annu. Rev. Earth Planet. Sci. 8, 205–230.

Brewer, J.A., Smythe, D.K., 1983. The Moine and Outer Isles Seismic Traverse (MOIST). In: Bally, A.W. (Ed.), Seismic Expression of Structural Styles. Am. Assoc. Petrol. Geol., Tulsa, Okla., 3, pp. 3.2.1.23–28.

Brewer, J.A., Matthews, D.H., Warner, M.R., Hall, J., Smythe, D.K., Whittington, R.J., 1983. BIRPS deep seismic reflection studies of the British Caledonides. Nature 305, 206–210.

Chávez-Pérez, S., Louie, J.N., 1995. Seismic reflection views of a blind thrust fault system using earthquake data. Society of Exploration Geophysicists 65th Annual Int. Meeting, Expanded Abstracts, Houston, Texas, October 8–13, pp. 511–514.

Chávez-Pérez, S., Louie, J.N., Pullammanappallil, S.K., 1996. Seismic depth imaging of normal faulting in the southern Death Valley basin. Society of Exploration Geophysicists 66th Annual Int. Meeting, Expanded Abstracts, Denver, Colo., November 10–15, II, pp. 1263–1266.

Chen, H.-w., McMechan, G.A., 1992. Effects of source configuration on seismograms. J. Seismic Explor. 1, 39–48.

Cook, F.A., Varsek, J.L., 1994. Orogen-scale décollements. Rev. Geophys. 32, 37–60.

Davis, T.L., Namson, J.S., 1994. A balanced cross-section of the 1994 Northridge earthquake, southern California. Nature 372, 167–169.

Donnellan, A., Hager, B.H., King, R.W., 1993. Discrepancy between geological and geodetic deformation rates in the Ventura basin. Nature 366, 333–336.

Fuis, G.S., Okaya, D.A., Clayton, R.W., Lutter, W.J., Ryberg, T., Brocher, T.M., Henyey, T.M., Benthien, M.L., Davis, P.M., Mori, J., Catchings, R.D., ten Brink, U.S., Kohler, M.D., Klitgord, K.D., Bohannon, R.G., 1996. Images of crust beneath southern California will aid study of earthquakes and their effects. EOS Trans. Am. Geophys. Union 77, 173–176.

Hadley, D., Kanamori, H., 1977. Seismic structure of the Transverse Ranges, California. Geol. Soc. Am. Bull. 88, 1469–1478.

Hale, D., Claerbout, J.F., 1983. Butterworth dip filters. Geophysics 48, 1033–1038.

Hauksson, E., 1990. Earthquakes, faulting, and stress in the Los Angeles basin. J. Geophys. Res. 95, 15365–15394.

Hauksson, E., 1994. The 1991 Sierra Madre earthquake sequence in southern California: Seismological and tectonic analysis. Bull. Seismol. Soc. Am. 84, 1058–1074.

Hauksson, E., Haase, J.S., 1997. Three-dimensional V_p and V_p/V_s velocity models of the Los Angeles basin and Central Transverse Ranges, California. J. Geophys. Res. 102, 5423–5453.

Hauksson, E., Jones, L.M., Hutton, K., 1995. The 1994 Northridge earthquake sequence in California: seismological and tectonic aspects. J. Geophys. Res. 100, 12335–12355.

Hauksson, E., Hafner, K., Clayton, R., 1996. Range of realistic velocity models for LARSE Line 1: from ray tracing and finite difference inversion techniques (abstract). EOS Trans. Am. Geophys. Union 77, Fall Meet. Suppl., F737.

Hedlin, M.A.H., Minster, J.-B., Orcutt, J.A., 1994. Resolution of prominent crustal scatterers near the NORESS small-aperture array. Geophys. J. Int. 119, 101–115.

Huang, W., Silver, L.T., Kanamori, H., 1996. Evidence for possible horizontal faulting in southern California from earthquake mechanisms. Geology 24, 123–126.

Huftile, G.J., Yeats, R.S., 1995. Convergence rates across a displacement tranfer zone in the western Transverse Ranges, Ventura basin, California. J. Geophys. Res. 100, 2043–2067.

Huftile, G.J., Yeats, R.S., 1996. Deformation rates across the Placerita (Northridge $M_w = 6.7$ aftershock zone) and Hopper Canyon segments of the western Transverse Ranges deformation belt. Bull. Seismol. Soc. Am. 86, S3–S18.

Ikelle, L.T., Kitchenside, P.W., Schultz, P.S., 1992. Parametrization of GRT inversion for acoustic and P–P scattering. Geophys. Prospect. 40, 71–84.

James, D.E., Clarke, T.J., Meyer, R.P., 1987. A study of seismic reflection imaging using microearthquake sources. Tectonophysics 140, 65–79.

Lay, T., 1987. Analysis of near-source contributions to early P-wave coda for underground explosions, III. Inversion for isotropic scatterers. Bull. Seismol. Soc. Am. 77, 1767–1783.

Lay, T., Young, C.J., 1996. Imaging scattering structures in the lower mantle by migration of long-period S waves. J. Geophys. Res. 101, 20023–20040.

Le Bras, R.J., Clayton, R.W., 1988. An iterative inversion of backscattered acoustic waves. Geophysics 53, 501–508.

Louie, J.N., Pullammanappallil, S.K., 1994. Seismic reflection inversions for the geometry of the Mojave segment of the San Andreas fault. Society of Exploration Geophysicists 64th Annual Int. Meeting, Expanded Abstracts, Los Angeles, Calif., October 23–28, pp. 964–967.

Louie, J.N., Clayton, R.W., Le Bras, R.J., 1988. 3-D imaging of steeply dipping structure near the San Andreas fault Parkfield, California. Geophysics 53, 176–185.

Lumley, D.E., Claerbout, J.F., Bevc, D., 1994. Anti-aliased Kirchhoff 3-D migration. Society of Exploration Geophysicists 64th Annual Int. Meeting, Expanded Abstracts, Los Angeles, Calif., October 23–28, pp. 1282–1285.

Lynnes, C.S., Lay, T., 1989. Inversion of P coda for isotropic scatterers at the Yucca Flat test site. Bull. Seismol. Soc. Am. 79, 790–804.

Magistrale, H., Zhou, H., 1996. Lithologic control of the depth of earthquakes in southern California. Science 273, 639–642.

Magistrale, H., McLaughlin, K., Day, S., 1996. A geology-based 3D velocity model of the Los Angeles basin sediments. Bull. Seismol. Soc. Am. 86, 1161–1166.

Matsumoto, S., 1995. Characteristics of coda waves and inhomogeneity of the earth. J. Phys. Earth 43, 279–299.

McCaffree, C.L., Christensen, N.I., 1993. Shear wave properties and seismic imaging of mylonite zones. J. Geophys. Res. 98, 4423–4435.

Meyer, R.P., James, D.E., 1987. Seismic reflection studies using

local earthquake sources. Geophys. J.R. Astron. Soc. 89, 27–34.

Morales, J., McMechan, G.A., 1990. Imaging of earthquake sources. Int. J. Imaging Syst. Technol. 2, 231–238.

Mori, J., Wald, D.J., Wesson, R.L., 1995. Overlapping fault planes of the 1971 San Fernando and 1994 Northridge, California earthquakes. Geophys. Res. Lett. 22, 1033–1036.

O'Brien, J.T., Kamp, W.P., Hoover, G.M., 1982. Sign-bit amplitude recovery with applications to seismic data. Geophysics 47, 1527–1539.

Pullammanappallil, S.K., Louie, J.N., 1993. Inversion of seismic reflection travel times using a nonlinear optimization scheme. Geophysics 58, 1607–1620.

Pullammanappallil, S.K., Louie, J.N., 1994. A generalized simulated-annealing optimization for inversion of first-arrival times. Bull. Seismol. Soc. Am. 84, 1397–1409.

Pullammanappallil, S., Louie, J.N., 1997. A combined first-arrival travel time and reflection coherency optimization approach to velocity estimation. Geophys. Res. Lett. 24, 511–514.

Revenaugh, J., 1995a. The contribution of topographic scattering to teleseismic coda. Geophys. Res. Lett. 22, 543–546.

Revenaugh, J., 1995b. A scattered-wave image of subduction beneath the Transverse Ranges, California. Science 268, 1888–1892.

Revenaugh, J., 1995c. Relation of the 1992 Landers, California, earthquake sequence to seismic scattering. Science 270, 1344–1347.

Revenaugh, J., Mendoza, H., 1996. Mapping shallow heterogeneity with teleseismic P to Rg scattered waves. Bull. Seismol. Soc. Am. 86, 1194–1199.

Rietbrock, A., Scherbaum, F., 1994. Acoustic imaging of earthquake sources from the Chalfant Valley, 1986, aftershock series. Geophys. J. Int. 119, 260–268.

Ryberg, T., Fuis, G.S., Lutter, W.J., Okaya, D.A., 1996. Mid- and upper-crustal structure of the San Gabriel Mountains: Results from the Los Angeles Seismic Experiment (LARSE) (abstract). EOS Trans. Am. Geophys. Union 77, Fall Meet. Suppl., F737.

Shaw, J.H., Suppe, J., 1996. Earthquake hazards of active blind-thrust faults under the central Los Angeles basin, California. J. Geophys. Res 101, 8623–8642.

Spudich, P., Bostwick, T., 1987. Studies of the seismic coda using an earthquake cluster as a deeply buried seismograph array. J. Geophys. Res. 92, 10526–10546.

Spudich, P., Iida, M., 1993. The seismic coda, site effects, and scattering in alluvial basins studied using aftershocks of the 1986 North Palm Springs, California, earthquake as source arrays. Bull. Seismol. Soc. Am. 83, 1721–1743.

Spudich, P., Miller, D.P., 1990. Seismic site effects and the spatial interpolation of earthquake seismograms: results using aftershocks of the 1986 North Palm Springs, California, earthquake. Bull. Seismol. Soc. Am. 80, 1504–1532.

Suppe, J., and Medwedeff, D.A., 1984. Fault-propagation folding (abstract). Geol. Soc. Am. 1984 Annu. Meet. Prog. Abstr., 16, 670.

Vidale, J.E., 1988. Finite-difference calculation of travel times. Bull. Seismol. Soc. Am. 78, 2062–2076.

Vidale, J.E., 1990. Comment on 'A comparison of finite-difference and Fourier method calculations of synthetic seismograms', by C.R. Daudt et al. Bull. Seismol. Soc. Am. 80, 493–495.

Webb, T.H., Kanamori, H., 1985. Earthquake focal mechanisms in the eastern Transverse Ranges and San Emigdio Mountains, southern California and evidence for a regional décollement. Bull. Seismol. Soc. Am. 75, 737–757.

Wu, R-S., 1989. Seismic wave scattering. In: James, D.E. (Ed.), The Encyclopedia of Solid Earth Geophysics. Van Nostrand Reinhold Co., New York, pp. 1166–1187.

Wu, R., Aki, K., 1985. Scattering characteristics of elastic waves by an elastic heterogeneity. Geophysics 50, 582–595.

Yeats, R.S., 1993. Converging more slowly. Nature 366, 299–301.

Zhao, D., Kanamori, H., 1995. The 1994 Northridge earthquake: 3-D crustal structure in the rupture zone and its relation to the aftershock locations and mechanisms. Geophys. Res. Lett. 22, 763–766.